







A Photovoltaic Self-Powered Volatile Organic Compounds Sensor Based on Asymmetric Geometry 2D MoS₂ Diodes

Mirette Fawzy,^{1,=}  Mohammad Reza Mohammadzadeh,^{2,=} Amin Abnavi,² Thushani De Silva,² Ribwar Ahmadi,² Hamidreza Ghanbari,² Fahmid Kabir,² Karen L. Kavanagh,¹ 
Amirhossein Hasani,^{3,z}  and Michael M. Adachi^{2,z} 

¹Department of Physics, Simon Fraser University, Burnaby V5A 1S6, British Columbia, Canada

²School of Engineering Science, Simon Fraser University, Burnaby V5A 1S6, British Columbia, Canada

³Department of Physics and MonArk NSF Quantum Foundry, Montana State University, Bozeman, Montana 59717, United States of America

Transition metal dichalcogenides have gained considerable interest for vapour sensing applications due to their large surface-to-volume ratio and high sensitivity. Herein, we demonstrate a new self-powered volatile organic compounds (VOC) sensor based on asymmetric geometry multi-layer molybdenum disulfide (MoS₂) diode. The asymmetric contact geometry of the MoS₂ diode induces an internal built-in electric field resulting in self-powering via a photovoltaic response. While illuminated by UV-light, the sensor exhibited a high responsivity of ~60% with a relatively fast response time of ~10 sec to 200 ppm of acetone, without an external bias voltage. The MoS₂ VOC diode sensor is a promising candidate for self-powered, fast, portable, and highly sensitive VOC sensor applications.

© 2024 The Author(s). Published on behalf of The Electrochemical Society by IOP Publishing Limited.. This is an open access article distributed under the terms of the Creative Commons Attribution 4.0 License (CC BY, <http://creativecommons.org/licenses/by/4.0/>), which permits unrestricted reuse of the work in any medium, provided the original work is properly cited. [DOI: 10.1149/2754-2726/ad7c61]



Manuscript submitted May 21, 2024; revised manuscript received September 11, 2024. Published October 7, 2024.

Supplementary material for this article is available [online](#)

Volatile organic compounds (VOCs) are highly reactive chemical compounds, that can evaporate into the air at ambient temperature and pressure.^{1,2} There are various sources of VOCs such as petroleum fuels, paints, cleaning products, pesticides, building materials and furnishings, and automobile exhaust.^{3,4} Exposure to VOCs can cause various adverse health effects such as skin irritation, impairment of the respiratory and nervous systems, and some VOCs are known to be carcinogenic, cause gene mutation, or are toxic to reproduction.⁵ Moreover, recent studies have shown that VOCs found in various human bodily fluids, including breath, sweat, urine, tears, saliva, and blood, can be considered as potential biomarkers for numerous health conditions and diseases. For instance, the presence of acetone in exhaled breath has been linked to diabetes, halitosis, and lung cancer.^{6,7} Breath acetone concentrations in healthy individuals typically range from 0.3 to 4 ppm but can rise as high as 1,250 ppm in adults experiencing diabetic ketoacidosis.⁸ By detecting VOCs, it is possible to use them as a screening tool to identify diseases in their early stages, when treatment options are more effective.⁹ Therefore, a portable sensor that can rapidly detect VOCs at low concentrations (e.g., parts-per-million (ppm) levels or lower) with high selectivity can be valuable in multiple areas including health management, environmental monitoring, and public safety.

Numerous methods exist for detecting VOCs, including electrical, optical, and gravimetric approaches.^{9–12} Among these, semiconductor metal oxides have been widely used in gas sensing due to their simple structure, production flexibility, and high sensitivity. However, many metal oxide semiconductor-based sensors require high operating temperatures, leading to significant power consumption.^{13–15} Additionally, existing VOC sensors typically rely on external power sources, making them incompatible with the low power and self-powered requirements of modern Internet of Things (IoT) devices such as smartphones and wireless sensing platforms.¹⁶ Thus, there is a need to develop efficient and convenient self-powered sensors capable of detecting VOCs at room temperature. Recent research has shown promising concepts for developing

self-powered VOC sensors that does not rely on external electrical energy to initiate the sensor-VOCs interaction or generate the readout signal.^{17,18} These sensors exhibit significantly lower power consumption compared to traditional sensors while also requiring less integration space.

Two-dimensional (2D) materials such as transition metal dichalcogenides (TMDs) have gained interest for sensing applications due to high carrier mobility and high sensitivity at room temperature attributed to their high surface to volume ratio.¹⁹ Nevertheless, studies on self-powered VOC sensors utilizing TMDs are limited. Photovoltaic self-powered sensors based on TMD p-n heterostructures have been recently reported for the detection of inorganic gases, NO₂ and NH₃.^{20,21} However, these heterostructures require complicated fabrication processes, which inevitably increase the complexity of processing and thus the production costs. Recent studies have shown that photovoltaic properties can be achieved in TMD devices by a simpler fabrication process, where metal contacts that are asymmetric in length and area are deposited onto the semiconducting channel.^{22–26} These geometrically asymmetric contact areas can result in a rectifying diode behavior even if the same metal is used on both sides. The diodes were also shown to exhibit photovoltaic properties and were used as self-driven photodetectors and solar cells. Moreover, it has been reported that varying the number of layers in exfoliated TMD flakes can tune the electronic properties and band structure, resulting in thickness-modulated homojunctions with photovoltaic properties.^{27,28} To the best of our knowledge, photovoltaic self-powered gas sensor using asymmetric geometry or thickness-modulated homostructure diodes has not yet been reported.

Herein, we have demonstrated a photovoltaic self-powered VOC sensor through the asymmetric geometry and thickness-modulated diodes based on exfoliated MoS₂ flakes for the first time. The sensor is self-powered via photovoltaic power generation under ultraviolet (UV) light illumination at room temperature. The as-fabricated devices show rectification properties with a sensitive and selective response toward three VOCs, acetone, ethanol, and IPA. Our device structure is simpler to achieve than conventional photovoltaic p-n junctions based on two different materials or those that require complicated doping mechanisms and fabrication processes.^{20,21,29} Moreover, owing to the high flexibility and mechanical stability of

⁼Equal Contribution.

^zE-mail: amirhossein.hasani@montana.edu; mmadachi@sfu.ca

MoS₂, our asymmetric MoS₂ VOC sensor holds great potential for flexible and portable VOC sensing devices with low power consumption.

Experimental

Fabrication of asymmetric geometry MoS₂ VOC sensors.—The detailed fabrication steps are illustrated in the schematic diagram of Fig. S1 (Supplementary Information). A p-type (100) Si wafer with resistivity ≤ 0.005 -ohm cm, coated with thermally oxidized 300 nm SiO₂, was used as the starting substrate. The substrates were first prepared through cleaning with acetone, 2-propanol, and deionized water for 10 min each in an ultrasonic bath. MoS₂ flakes were mechanically exfoliated from a bulk MoS₂ crystal (SPI supplies) using tape (Nitto SPV224) and transferred onto the cleaned SiO₂/Si substrates. Suitable flakes were identified by optical microscopy and chosen for their triangular shapes or sharp angles and irregular thicknesses. In addition to selecting flakes with triangular and asymmetric shapes, we targeted a thickness range of 20 nm to 60 nm to optimize the rectification ratio and photovoltaic performance of the fabricated device.^{25,26} Contacts were patterned on the chosen asymmetric MoS₂ flakes, using standard photolithography, such that the contact length and area varied between the two sides of the metal-semiconductor interface. During the lithography process, photoresist (Microposit S1813) was spin-coated onto the substrate at 3000 rpm for 30 s. The substrate then underwent a one-minute soft-bake on a hotplate at 100 °C. Following this, the electrodes were patterned by exposing the coated photoresist to 365 nm UV light through a shadow mask for 7 s. The process was completed by developing the photoresist (Microposit MF-319 developer) for 20 s. Layers of Cr (10 nm) followed by Au (60 nm) were subsequently deposited through thermal evaporation followed by lift-off in an acetone bath.

Device characterizations.—The thickness of the MoS₂ flake was measured using atomic force microscopy (MFP-3D AFM, Asylum Research, Santa Barbara). The Raman spectroscopy measurements were obtained using a confocal Raman microscope (Renishaw inVia) under a 514 nm continuous-wave excitation laser. The electrical and photovoltaic characteristics of the asymmetric MoS₂ VOC sensor were measured using a semiconductor characterization system connected to a probe station (Keithley 4200-SCS) at room temperature. The power density of the UV light source was modulated by a power supply and calibrated by a silicon photodiode sensor (Thorlabs, USA, S120VC).

VOC sensing measurements.—A home-built vapour sensing setup was used to perform all the VOC sensing tests, as illustrated in Figure S8 (Supplementary Information). The sensor was mounted, using tungsten probes, inside an enclosed chamber stage (Linkam, HFS350EV-PB4) that is connected to the outlet of a gas sampling bulb. N₂ was used as the carrier gas, and it was passed through the inlet of the gas sampling bulb using a flow controller. A measured volume of each liquid VOC was injected into the gas sampling bulb using a syringe to obtain the desired VOC concentrations. The gas sampling bulb was placed on a hot plate to generate the required VOCs vapor. The different VOC concentrations were calculated using the following formula:

$$C_{ppm} = \frac{T \times \rho \times R \times V_{Liquid}}{M_{Liquid} \times P_{Chamber} \times V_{Chamber}} \times 10^6 \quad [1]$$

where C_{ppm} is the desired target VOC concentration in parts per million (ppm), T (K) is the absolute temperature, ρ (g/mL) is the density of the liquid VOC, R is the universal gas constant, V_{Liquid} is the volume of the injected liquid VOC (mL), M (kg/mol) is the molecular weight of the liquid VOC, $P_{Chamber}$ (kPa) is the pressure inside the chamber, and $V_{Chamber}$ (mL) is volume of the chamber. Before injecting the desired

VOC, the sensors were left to stabilize for 15 min. All the sensing measurements were performed at room temperature (~ 25 °C) under UV illumination with a power density of 26.4 mW cm⁻². No external bias was applied to the sensors, and a UV LED lamp with a wavelength of 365 nm was fixed above the top window of the VOC sensing chamber to directly illuminate the sensor. The real-time current output signal was measured using a Keithley 2400 source meter. The response time was calculated as the time required for the sensor response to reach 90% of the maximum signal, and the recovery time was the time required for the sensor to return to 10% of the original baseline signal in the absence of the target VOC.

Results and Discussion

VOC sensor characterization.—Multilayer 2H-phase semiconducting MoS₂ flakes were used as the active sensing material. Figure 1a shows a schematic illustration and optical image of a typical asymmetric geometry MoS₂ diode. The MoS₂-Cr contact areas are 2000 μm^2 and 171 μm^2 , resulting in a MoS₂-Cr contact area difference of 1829 μm^2 . Similarly, the lengths of the MoS₂-Cr interfaces are 96 μm and 16 μm , resulting in a MoS₂-Cr interface length difference of 75 μm . The MoS₂ regions under the two metal contacts also have slightly different thicknesses as seen in Fig. S2 (Supplementary Information). An atomic force microscopy (AFM) image of the device in Fig. 1b shows a MoS₂ flake with an average thickness of 55.5 ± 0.4 nm (up to 78 layers of MoS₂) in the uniform middle area of the flake (further away from the contacts). In Fig. 1c, the characteristic Raman modes of the in-plane E_{2g} (383.999 cm⁻¹) and out-of-plane A_{1g} (406.331 cm⁻¹) are observed, confirming that the exfoliated MoS₂ flakes are 2H-MoS₂ semiconducting crystals.³⁰ The reported peaks in the literature for multilayer MoS₂ crystals are 382 cm⁻¹ and 407 cm⁻¹, corresponding to the in-plane E_{2g} and out-of-plane A_{1g} modes, respectively.³¹⁻³⁵

Electrical measurements and photovoltaic properties of the sensor.—The optoelectronic performance of the fabricated devices was characterized under dark and UV light illumination (peak wavelength $\lambda = 365$ nm), as illustrated in the diagram in Fig. 2a. The metal electrode with the smaller contact area was grounded, while a bias voltage was applied to the larger contact area electrode. Figure 2b shows the I-V curves of the asymmetric geometry diode in the dark and under UV illumination at different power densities. The J-V characteristics of the device under dark and UV-light conditions with a light intensity of 26.4 mW cm⁻² is shown in Fig. 2c. Under dark conditions, the diode showed excellent diode rectifying behavior, with a rectification ratio (defined as the current ratio at 1 V and -1 V) of 10⁴ in the absence of any gate voltage modulation, which is among the highest value of all previously reported diodes based on geometrically-asymmetric 2D materials.^{22,23,25,36,37}

This observed diode rectification behavior is attributed to unequal Schottky barriers and/or depletion volumes between the two MoS₂-metal interfaces, likely associated with variable degrees of sulfur diffusion and interfacial electron accumulation.^{23,25,26,38} To confirm and quantify the Schottky barrier height difference at the two metal-semiconductor interfaces across the flake, the surface potential across the area of an asymmetric device was measured using Kelvin probe force microscopy (KPFM) shown in Fig. S3 (Supplementary Information). The surface potential measured across the larger and smaller contact regions, fabricated with the same metal (Cr), shows a difference in surface potential at both sides of the flake arising from barrier height differences from the different contact areas. An additional factor that influences the barrier height is the difference in MoS₂ thickness at the two metal contacts.³⁹⁻⁴¹ This thickness modulation may be contributing to the asymmetric transport observed in Figs. 2b and 2c, which agrees with previous reports.²³ The mechanical exfoliation method produces flakes with a random distribution of size, thickness, and shape. However, high diode rectification was repeatedly observed in multiple fabricated

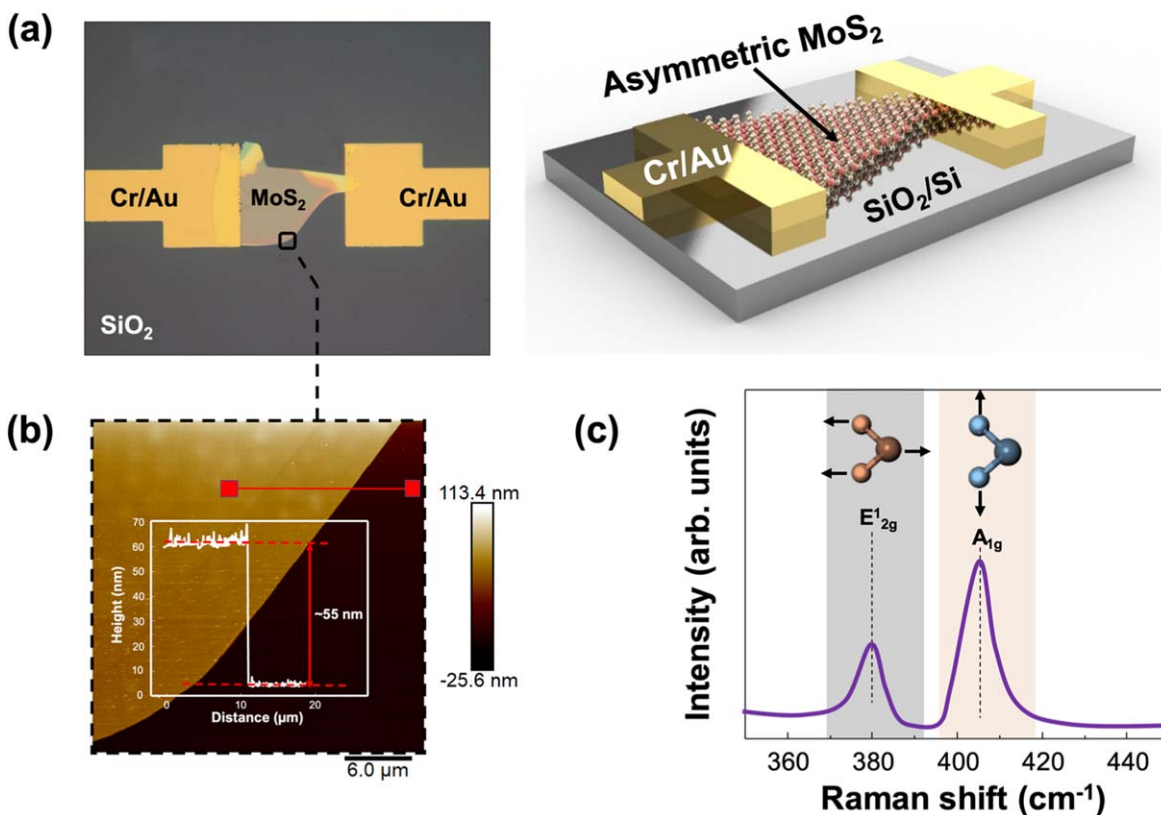


Figure 1. Structural characterization of the asymmetric geometry MoS₂ device. (a) Schematic illustration and optical micrograph of the device. (b) AFM image and the corresponding height profile of the MoS₂ flake. (c) Raman spectra of the 2H-MoS₂ crystal.

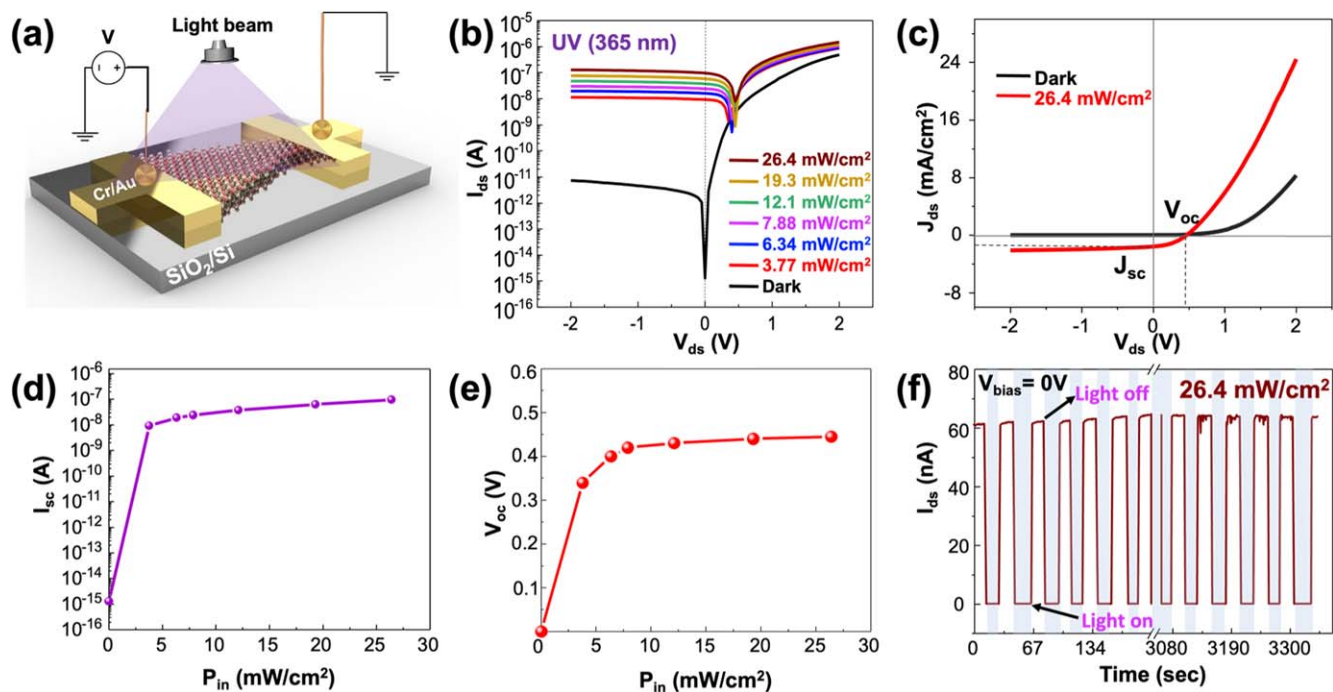


Figure 2. Photovoltaic properties of the asymmetric geometry MoS₂ diode. (a) Schematic of the device under UV-light illumination. (b) I-V curves of the device under UV-light illumination with different power intensities, (c) J-V characteristics of the device under UV-light illumination and dark conditions, (d) I_{sc} and (e) V_{oc} of the device as a function the light intensity, and (f) the photodynamic response of the device under UV-light illumination (26.4 mW cm⁻²) at 0 V bias. The shaded (unshaded) regions represent when the illumination is ON (OFF).

asymmetric geometry MoS₂ diodes. Figure S4 (Supplementary Information) shows examples of four asymmetric geometry MoS₂ devices with rectification ratios ranging from 10² to 10⁴. No significant rectification was observed for MoS₂ flakes with symmetric geometries as shown in Fig. S5 (Supplementary Information).

When the asymmetric diodes are illuminated, photoinduced electron–hole pairs are generated within the MoS₂ active layer, causing the reverse current density to increase (Fig. 2b). The photocurrent increases with increasing illumination power density due to the photogeneration of more electron–hole pairs that are separated and collected by the applied reverse bias voltages.⁴² At zero bias voltage, the asymmetric built-in electric field at the metal–semiconductor junctions generates a photogenerated short-circuit current (I_{sc}).²² The short-circuit current density and open-circuit voltage (V_{oc}) increase as a function of increasing incident UV illumination reaching 1.58 mA cm⁻² and 450 mV, respectively, at the highest power density of 26.4 mW cm⁻² (Figs. 2d and 2e). To demonstrate repeatability of photogenerated charge collection using the asymmetric geometry architecture, the I–V characteristics and photovoltaic performance of six other MoS₂ diodes with different geometric shapes are shown in Fig. S6 (Supplementary Information). The photodynamic response of an asymmetric diode at zero bias voltage is presented in Fig. 2f.

The photocurrent switching under the highest intensity illumination was tested, and the device was found to be stable for over 3000 cycles of ON/OFF light switching, thus confirming the stable and repeatable photovoltaic performance of the fabricated asymmetric geometry devices. Similar photocurrent switching behavior was measured for other asymmetric devices, some of which are presented in Fig. S7 (Supplementary Information).

VOCs sensing properties.—Based on the exhibited photovoltaic effect, the devices were tested to detect VOCs in the absence of external bias voltage. Figure 3 illustrates the VOC sensing performance of an asymmetric diode when exposed to three different VOCs under zero applied bias. Figures 3a–3c show the time-dependent current responses of the sensor to acetone, ethanol, and 2-propanol, respectively. Each VOC was introduced at five different concentrations (20, 50, 100, 150, and 200 ppm (parts per million)). The VOC sensing response (%) of the devices was calculated using the following equation:

$$\text{Response}(\%) = \frac{I_g - I_0}{I_0} \times 100 = \frac{\Delta I}{I_0} \times 100 \quad [2]$$

where I_0 is the short-circuit current in absence of any VOCs, and I_g refers to the corresponding short-circuit current when exposed to the target VOC. The positive sensing response for acetone increased monotonically from 7% (20 ppm) to 60% (200 ppm) with good recovery at room temperature when compared to other self-powered sensors based on 2D materials.^{20–22} The sensor showed a similar increasing response when exposed to ethanol (Fig. 3b) and 2-propanol (Fig. 3c), but a different response trend was observed for each VOC. To evaluate those trends, the response of the sensor to the three VOCs as a function of VOC concentration is plotted in Fig. 3d. As illustrated in Fig. 3d, the sensor's response to acetone increases sharply with concentration, while 2-propanol experiences a slower rise in response, and ethanol's response flattens after reaching 100 ppm. The response of gas sensors is a crucial parameter that reflects the underlying physical and chemical interactions between the sensor material and the analyte. In VOC sensors, this response is shaped by a complex interplay of adsorption/desorption kinetics, the physical and chemical properties of VOCs, and environmental factors. These parameters can cause variations in sensor response trends, even under identical experimental conditions. These differences are valuable for selectively detecting target gases. For instance, Mohammadzadeh et al. employed photo-excited 2D GeS crystals to produce unique time-resolved electrical responses, using

machine learning to identify VOCs based on these distinct fingerprints, thereby enhancing selective detection.¹ Similarly, Acharyya et al. demonstrated that a tin oxide-based sensor could effectively discriminate between multiple VOCs using gas sensing kinetic analysis. They used the Eley-Rideal model to obtain unique kinetic properties for each VOC.⁴³

The transient response to acetone at 200 ppm exhibited a fast response time of around 10 sec and a recovery time of 140 sec as shown in Fig. 3e. Key figures of merit for the sensor were calculated, including a sensitivity of 96.15 pA/ppm and a limit of detection (LOD) of 1.113 ppm for acetone, to which the sensor showed the highest response. The corresponding results for 2-propanol and ethanol are provided in Table S1 (Supplementary Information).

To examine the sensor's response to different VOCs, the sensor was exposed to three additional VOCs: toluene, hexane, and butanone (Fig. 3f). Each VOC was introduced at a concentration of 200 ppm. The sensor showed the highest sensitivity towards acetone at this concentration which agrees with previous studies on MoS₂ VOC sensors.^{44,45} The reproducibility of the VOC sensor was evaluated through multiple repeated measurements, as shown in Fig. S9 (Supplementary Information). The sensor's responses to ethanol and butanone at concentrations of 50, 100, and 200 ppm were recorded, with each bar representing the average response across four consecutive exposures. Error bars reflect the standard deviation for each set of exposures. The coefficient of variation (CV) was calculated to be 12% for butanone and 10% for ethanol, indicating a high level of consistency and reproducibility in the sensor's performance across different exposure levels. The obtained CV values are also below the 20% threshold suggested by the EPA for low-cost air quality sensors.^{46,47}

The effect of relative humidity, an important environmental factor on the sensor response, is also shown in Fig. S10 (Supplementary Information). The sensor response to 100 ppm of Acetone under UV light illumination at an intensity of 26.4 mW cm⁻² and zero bias decreased as the relative humidity (RH) increased from 20% to 90% at room temperature. Water molecules likely occupied available active sites and act as a barrier between the VOC molecules and the surface, lowering the device's responsivity toward the target VOC. The observed effect agrees with the results previously reported for 2D material-based gas sensors.¹ Unfortunately, for room-temperature gas sensors, addressing humidity interference remains a significant hurdle for practical application.

VOCs sensing mechanism.—The VOCs sensing characteristics of 2D-based sensors is attributed to the charge transfer mechanism induced by the physisorption of the VOC molecules over the surface of the active layer. The mechanism of photovoltaic self-powered VOC sensing can be explained by electronic band diagrams of the asymmetric geometry devices. Figures 4a, 4c, and 4e show schematic illustrations of the sensor under UV-light illumination in three conditions, namely (I) symmetric MoS₂, (II) asymmetric MoS₂, and (III) asymmetric MoS₂ exposed to VOCs. The corresponding band diagrams between the MoS₂ and Cr/Au are illustrated in Figs. 4b, 4d, and 4f, respectively, where ϕ_1 and ϕ_2 are the barrier heights at the two MoS₂–Cr electrode interfaces. The electronic barrier heights are equal in the symmetric geometry device (Fig. 4b), whereas for the asymmetric geometry device (Fig. 4d), the barrier height of the larger MoS₂–Cr interface, ϕ_1 , is higher than ϕ_2 and the width of the depletion region is increased by changing the geometry of MoS₂ from symmetric to asymmetric. This is due to the unequal geometry of the MoS₂–Cr interface near the Cr/Au contact area which generates a nonuniform internal electric field.³⁶ When the asymmetric geometry MoS₂ device is exposed to VOCs under light illumination (Fig. 4f), there are more injected electrons from VOC molecules, resulting in an increase in photocurrent. During the sensor testing, the VOCs act as electron donors leading to a change in the carrier concentration of the MoS₂ nanosheet.¹

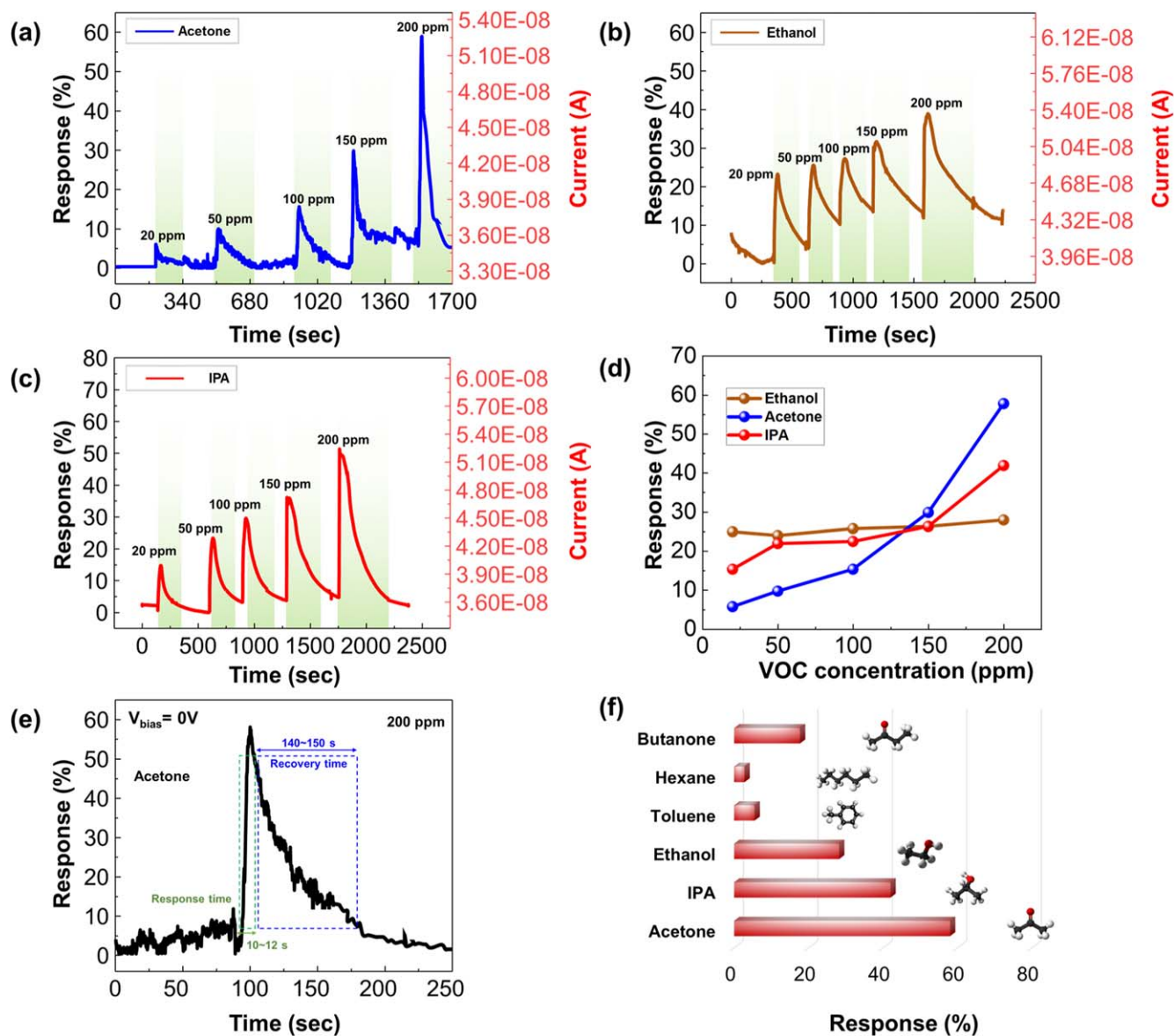


Figure 3. VOCs sensing properties of the asymmetric geometry MoS₂ sensor. Device response (%), left axis and current (A), right axis at zero bias voltage and under UV-light illumination exposed to different concentrations of (a) acetone, (b) ethanol, and (c) IPA. (d) Comparison of the sensor response as a function of acetone, ethanol, and IPA concentrations from 20 to 200 ppm under UV-light illumination at zero bias voltage. (e) Enlarged plot showing the sensor response time (10–12 s) and recovery time (140–150 s) to 200 ppm of acetone at zero bias voltage and under UV-light illumination. (f) Amplitude of sensor response under UV-light illumination at zero bias to different VOCs each at 200 ppm. The light green bars in (a), (b), and (c) represent the combined response and recovery times of the device at each concentration.

VOC sensor performance.—To assess the performance of our asymmetric geometry VOC sensor relative to other self-powered sensors, we have summarized recent studies on various self-powered VOC sensors operating at room temperature in Table I. Compared to self-powered gas sensors that rely on piezoelectric or triboelectric principles, photovoltaic-based sensors eliminate the need for additional mechanical energy.

Most photovoltaic-based gas sensors achieve self-powered operation or function without an applied bias by forming a p-n junction. For instance, Hoffmann et al. developed a self-powered VOC sensor by combining gas sensing (CdS@n-ZnO) with solar energy harvesting (n-ZnO/p-Si diode) in a single structure.⁵⁴ Other self-powered gas sensors based on 2D materials have employed the stacking of different materials to create p-n vertical heterostructures, including combinations such as MoS₂/WSe₂, WS₂/WSe₂, MoS₂/GaSe, and MoS₂/Te.^{20,21,29} Although some of the previously mentioned studies report improved sensing capabilities, particularly

for inorganic gases NO₂ and NH₃, the fabrication of p-n diodes necessary for self-powered operation involves complicated fabrication steps, leading to higher production costs. Our asymmetric-geometry diode sensor offers a sensing response on par with the self-powered VOC sensors mentioned, while being easy to fabricate using metal-semiconductor Schottky diodes.

Additionally, we further evaluated our sensor's performance by comparing it with other non-self-powered 2D MoS₂-based VOC sensors, as shown in Table II. 2D MoS₂ is a highly promising sensing material due to its large surface-to-volume ratio and abundant active sensing sites.⁵⁵ However, as seen in Table II, existing strategies for using 2D MoS₂ to detect volatile organic compounds (VOCs) face certain limitations, including high operating temperatures,^{56–59} low gas sensitivity, and complex fabrication processes that require using expensive materials. For example, several studies have involved functionalizing or decorating the MoS₂ surface with metals like Au and Pt to improve its sensing

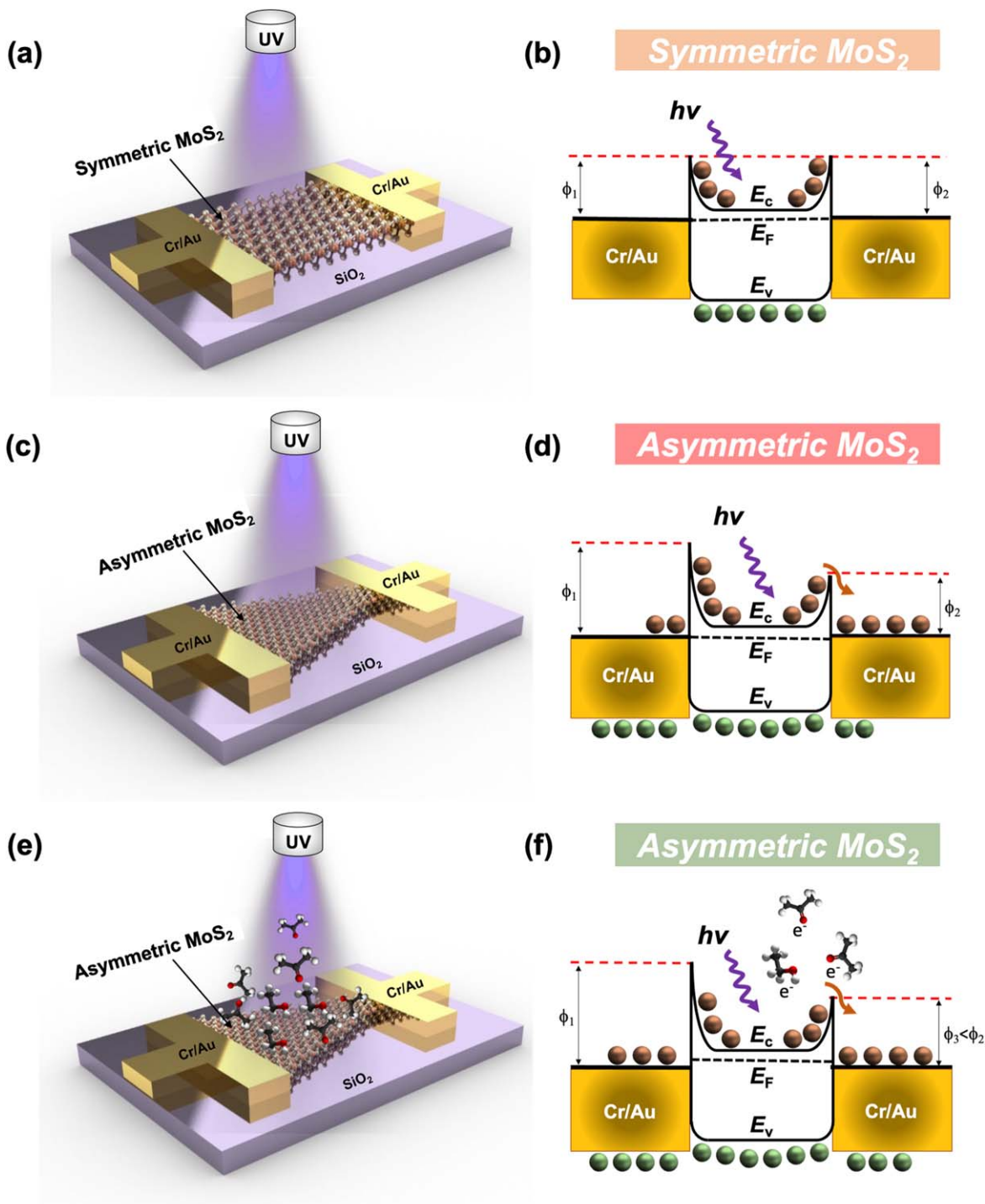


Figure 4. Sensing mechanism of the VOC sensor. Schematics of MoS₂ devices under UV-light illumination with their corresponding band diagrams: (a) and (b) symmetric, (c) and (d) asymmetric, and (d) and (e) asymmetric exposed to VOCs.

properties.^{57,59,60} These challenges hinder the development of effective room-temperature gas sensors. As seen in Table II, our VOC sensor operates at room temperature with high sensitivity, without requiring costly metals or complex fabrication steps.

Another critical factor to assess for our sensors is their reproducibility and scalability potential. The performance of the asymmetric geometry VOC sensor is affected by the electrical and photovoltaic properties of the asymmetric diode. Typically, the rectification factor, and consequently the photovoltaic characteristics, are enhanced in triangular-shaped flakes that exhibit significant asymmetry in the metal-MoS₂ overlap area between the two

contacts. In this study, mechanically exfoliated flakes were used to demonstrate the self-powered VOC detection method. For commercial applications, precise lithographic control over flake geometry will be essential to produce reproducible and reliable sensors with scalable potential.

By employing a large-area compatible process for preparing thin MoS₂ films,⁶² the sensing area can be patterned into regular triangular shapes through lithography and etching, allowing for better control over the flake geometry. For example, large-area graphene oxide films patterned into asymmetric geometries have demonstrated diode behavior and have been successfully used as pH sensors.⁶³ With

Table I. Room-temperature self-powered VOC sensing performance: comparison of our sensor with reported sensors.

Device structure	Target VOC	Detection range (ppm)	Response (%) ^{a)}	Mechanism	References
ZnO Nanowires	Ethanol	100–700	27.5	Piezoelectric	48
Pd/ZnO Nanoarray	Ethanol	200–800	16	Piezoelectric	49
Pt/ZnO Nanoarray	Ethanol	400–1500	6	Piezoelectric	50
Au/ZnO Nanoarray	Ethanol	400–1200	2.5	Piezoelectric	51
α -Fe ₂ O ₃ /ZnO Nanowires	Ethanol	100–700	28.3	Piezoelectric	52
PANI/PTFE/PANI	Ethanol	30–210	66.8	Triboelectric	53
	Methanol		79.5		
	Propanol		55.4		
	Chloroform		74.7		
CdS@n-ZnO/p-Si	Butanol	50–200	47.1	Photovoltaic	54
	Ethanol		6.5		
Asymmetric Geometry 2D MoS ₂	Acetone	20–200	60	Photovoltaic	This Work
	2-Propanol		51		
	Ethanol		43		

a) The responses above were calculated at a concentration of 200 ppm except for the devices with a detection range starting from 400 ppm. Their response was evaluated at 400 ppm.

Table II. Comparison of VOC sensing performance of 2D MoS₂-based structures.

Sensor structure	Tested VOCs	Operating temperature (°C)	Response (%) [VOC, concentration]	Response/recovery time (sec)	Self-powered	References
Dual Channel MoS ₂	Acetone	100 °C	3	—	N	56
	Ethanol		[Acetone, 3000 ppm]			
	Toluene					
Pt-functionalized MoS ₂ paper	Acetone	50 °C	33	180–365	N	57
	Ethanol		[Acetone, 100 ppm]			
	Methanol					
	2-propanol					
Pristine MoS ₂	Toluene	110 °C	25	—	N	58
	Xylene					
	Benzene					
Au-functionalized MoS ₂	Ethanol	RT	[Ethanol, 500 ppm]	—	N	60
	Acetone		31.6			
	2-propanol		[Acetone, 40 ppm]			
	Toluene					
La@MoS ₂	Benzene	RT	20.1	48.5/43.2	N	61
	Acetone					
	Chloroform					
	Ethanol					
	Isopropanol					
MoS ₂ /GaSe	Methanol	RT	5	—	Y	21
	Ethanol		[Ethanol, 500 ppm]			
	Acetone					
Au-decorated MoS ₂	Acetone	150 °C	29	—	N	59
	Ethanol		[Acetone, 50 ppm]			
	Acetaldehyde					
Au-doped MoS ₂	Acetone	RT	6	180/240	N	44
	Ethanol		[Acetaldehyde, 1000 ppm]			
	Hexane					
	Toluene					
	Acetone					
Asymmetric Geometry MoS ₂	Ethanol	RT	60	10/140	Y	This work
	2-Propanol		[Acetone, 200 ppm]			
	Butanone					
	Hexane					
	Toluene					

advancements in large area 2D material synthesis, scaling up the fabrication process for diode-based VOC sensors is possible.

Conclusions

In summary, a self-powered VOC sensor based on an asymmetric geometry MoS₂ diode was demonstrated for the first time. The as-fabricated devices exhibited a rectification ratio of 10⁴ in the absence of any gate voltage modulation presumably due to the built-in electric field. In addition, the VOC sensor showed a response of 60% and a fast response time of 10 sec to 200 ppm of acetone without an external bias voltage. Therefore, a VOC sensor based on this asymmetric MoS₂ diode could be a promising candidate for fast, portable, highly sensitive, and low power monitoring systems.

Acknowledgments

This work was supported with Natural Sciences and Engineering Research Council (NSERC) [RGPIN-2017-05810 and ALLRP 590618-23], Western Economic Diversification Canada (WD) [Project No. 000015280], New Frontiers in Research Fund (NFRF) —Exploration [NFRFE-2018-00214], Canada Foundation for Innovation (CFI) [Project No. 38331], British Columbia Knowledge Development Fund (BCKDF) [Project No. 38331], WorkSafeBC [RS2021-SP09]. The authors thank B. Kim for supporting the SFU Engineering Science cleanroom and Dr. D. Leznoff for access to Raman Spectroscopy instrumentation. The authors acknowledge CMC Microsystems and 4D LABS shared facilities that facilitated this research.

ORCID

Mirette Fawzy  <https://orcid.org/0000-0003-0430-9489>
 Karen L. Kavanagh  <https://orcid.org/0000-0002-3059-7528>
 Amirhossein Hasani  <https://orcid.org/0000-0003-0965-4169>
 Michael M. Adachi  <https://orcid.org/0000-0003-3015-2606>

References

- M. R. Mohammadzadeh et al., *Adv. Sci.*, **10**, 2205458 (2023).
- J. Zhu, Z. Ren, and C. Lee, *ACS Nano*, **15**, 894 (2021).
- Z. Du, S. Zhang, J. Li, N. Gao, and K. Tong, *Appl. Sci.*, **9**, 338 (2019).
- K. Zhao et al., *Nano Energy*, **53**, 898 (2018).
- Y. Saalberg and M. Wolff, *Clin. Chim. Acta*, **459**, 5 (2016).
- A. H. Jalal et al., *ACS Sens.*, **3**, 1246 (2018).
- M. Shirasu and K. Touhara, *J. Biochem. (Tokyo)*, **150**, 257 (2011).
- J. C. Anderson, *Obesity*, **23**, 2327 (2015).
- M. Khatib and H. Haick, *ACS Nano*, **16**, 7080 (2022).
- V. Galstyan et al., *Rev. Anal. Chem.*, **40**, 33 (2021).
- S. Khan, S. Le Calvé, and D. Newport, *Sens. Actuators Phys.*, **302**, 111782 (2020).
- C. K. McGinn, Z. A. Lampert, and I. Kymissis, *ACS Sens.*, **5**, 1514 (2020).
- A. Mirzaei, S. G. Leonardi, and G. Neri, *Ceram. Int.*, **42**, 15119 (2016).
- T. Lin, X. Lv, Z. Hu, A. Xu, and C. Feng, *Sensors*, **19**, 233 (2019).
- S. D. Lawaniya, A. Awasthi, P. W. Menezes, and K. Awasthi, *Adv. Sens. Res.*, **n/a**, 2400101 (2024).
- Z. Song et al., *ACS Nano*, **15**, 7659 (2021).
- X.-L. Liu et al., *IEEE Sens. J.*, **21**, 5628 (2021).
- G. Khandelwal and R. Dahiya, *Adv. Mater.*, **34**, 2200724 (2022).
- W. C. Tan and K.-W. Ang, *Adv. Electron. Mater.*, **7**, 2001071 (2021).
- Y. Kim et al., *Adv. Funct. Mater.*, **30**, 2003360 (2020).
- Y. Niu et al., *Adv. Sci.*, **8**, 2100472 (2021).
- C. Zhou et al., *Adv. Funct. Mater.*, **28**, 1802954 (2018).
- W. Gao et al., *Adv. Electron. Mater.*, **7**, 2000964 (2021).
- J. Chen et al., *Adv. Mater. Interfaces*, **9**, 2200075 (2022).
- A. Abnavi et al., *Adv. Funct. Mater.*, **33**, 2210619 (2023).
- T. De Silva et al., *Nat. Commun.*, **13**, 7593 (2022).
- H. Xia et al., *Light: Sci. Appl.*, **11**, 170 (2022).
- B. Yarrow, A. M. Askar, A. M. Parameswaran, and M. M. Adachi, *ACS Appl. Electron. Mater.*, **1**, 2150 (2019).
- M. R. Mohammadzadeh et al., *Small*, **n/a**, 2402464 (2024).
- A. Abnavi et al., *ACS Appl. Mater. Interfaces*, **13**, 45843 (2021).
- L. Liang and V. Meunier, *Nanoscale*, **6**, 5394 (2014).
- C. Lee et al., *ACS Nano*, **4**, 2695 (2010).
- Y. Yu et al., *Sci Rep.*, **3**, 1866 (2013).
- Y.-H. Lee et al., *Nano Lett.*, **13**, 1852 (2013).
- N. A. Lanzillo et al., *Appl. Phys. Lett.*, **103**, 093102 (2013).
- G. Dushaq and M. Rasras, *ACS Appl. Mater. Interfaces*, **13**, 21499 (2021).
- J. Lu et al., *Nanoscale*, **12**, 7196 (2020).
- M. D. Siao, W. C. Shen, R. S. Chen, Z. W. Chang, M. C. Shih, Y. P. Chiu, and C.-M. Cheng, *Nat. Commun.*, **9**, 1442 (2018).
- M. Tosun et al., *Sci Rep.*, **5**, 10990 (2015).
- H. S. Lee et al., *Nano Lett.*, **12**, 3695 (2012).
- S. Qiao et al., *ACS Appl. Mater. Interfaces*, **9**, 18377 (2017).
- H.-Y. Chen et al., *J. Mater. Chem. C*, **2**, 9689 (2014).
- S. Acharyya et al., *ACS Sens.*, **6**, 2218 (2021).
- S.-Y. Cho, H.-J. Koh, H.-W. Yoo, J.-S. Kim, and H.-T. Jung, *ACS Sens.*, **2**, 183 (2017).
- J.-S. Kim, H.-W. Yoo, H. O. Choi, and H.-T. Jung, *Nano Lett.*, **14**, 5941 (2014).
- R. Williams, V. Kilaru, E. Snyder, A. Kaufman, T. Dye, A. Rutter, and A. Russell, *Air Sensor Guidebook* (2014).
- M. Justo Alonso et al., *Build. Environ.*, **222**, 109380 (2022).
- P. Wang et al., *J. Mater. Chem. A*, **3**, 3529 (2015).
- Y. Lin et al., *Nanoscale*, **6**, 4604 (2014).
- Y. Zhao et al., *Nanotechnology*, **25**, 115502 (2014).
- L. Xing et al., *Appl. Phys. Lett.*, **104**, 013109 (2014).
- D. Zhu et al., *Mater. Lett.*, **166**, 288 (2016).
- X. Xue, Y. Fu, Q. Wang, L. Xing, and Y. Zhang, *Adv. Funct. Mater.*, **26**, 3128 (2016).
- M. W.-G. Hoffmann et al., *Nano Energy*, **2**, 514 (2013).
- R. Kumar, W. Zheng, X. Liu, J. Zhang, and M. Kumar, *Adv. Mater. Technol.*, **5**, 1901062 (2020).
- E. Kuş et al., *Nanomaterials*, **14**, 633 (2024).
- R. Bhardwaj, V. Selamneni, U. N. Thakur, P. Sahatiya, and A. Hazra, *New J. Chem.*, **44**, 16613 (2020).
- J. M. Suh et al., *Electron. Mater. Lett.*, **15**, 368 (2019).
- T. Kim et al., *ACS Nano*, **17**, 4404 (2023).
- W. Y. Chen, C.-C. Yen, S. Xue, H. Wang, and L. A. Stanciu, *ACS Appl. Mater. Interfaces*, **11**, 34135 (2019).
- K. Rathi, A. N. Kumar, and K. Pal, *Nanotechnology*, **31**, 395504 (2020).
- T. Li et al., *Nat. Nanotechnol.*, **16**, 1201 (2021).
- M. Miansari, J. R. Friend, and L. Y. Yeo, *Adv. Sci.*, **2**, 1500062 (2015).